Frictional aging, de-aging, and re-aging in a monolayer-coated micromachined interface

Alex D. Corwin* and Maarten P. de Boer†
MEMS Technology Department, Sandia National Laboratories, Albuquerque, New Mexico 87185, USA
(Received 23 January 2009; published 12 May 2010)

Measurements on monolayer-coated polycrystalline silicon surfaces have shown that the static friction coefficient μ_s strongly depends on loading parameters including hold time and normal hold force by Corwin and de Boer [J. Microelectromech. Syst. **18**, 250 (2009)]. In that work, μ_s was measured by keeping the tangential force constant and lowering normal force until motion occurred. Results indicated that μ_s also depends strongly on normal force ramp-down rate. Here, we postulate that if the normal load is lowered instantaneously, the time for the block to begin moving, the "release time" t_r, will be greater than the inertial response time, which is on the order of 5 μs. We measure the release time and find that it spans nearly six decades from less than 100 μs to almost 50 s. Release time depends on the loading and unloading history through all three of the parameters varied: hold time, hold force, and release force. An empirical model incorporating all three of these parameters fits the release time data over the full range. Release time decreases after the contacting surfaces are held together at increasing hold force levels and this *qualitatively* explains a previous observation that static friction aging is suppressed with increasing normal force at a fixed tangential load in this interfacial system. We further *quantitatively* relate the previous μ_s loading dependence on all three parameters to the release time model established here by introducing a "re-aging" parameter. This work firmly establishes that release time is a more fundamental parameter than the static friction coefficient and is the origin of static friction coefficient dependencies in this micromachined interface.

DOI: 10.1103/PhysRevB.81.174109 PACS number(s): 62.20.Qp, 46.55.+d, 81.40.Pq

I. INTRODUCTION

Understanding dry friction has long been a subject of scientific and engineering investigation at the macroscale.[1] Most often, friction occurs between surfaces that are rough. As shown by Bowden and Tabor,[2] an applied normal force F_n is borne by high points, or asperities, on the surfaces and the real contact area is much smaller than the apparent area. If the asperities are plastically deformed, the real contact area is proportional to the pressure. Even if the surfaces are elastically deformed, the same result holds,[3] provided that there is a continuous supply of fresh asperities as normal force increases. By assuming a constant shear strength of the contacting asperities, Amontons' empirically determined law of static friction, $F_s=\mu_s F_n$, where F_s is the static friction force and μ_s the static coefficient of friction, can be derived.

Many studies have shown Amontons' law is only a first approximation for so-called multicontact interfaces. An empirical formulation known as rate-and-state friction has evolved to incorporate logarithmic aging and memory effects. Rock was first studied to understand earthquake phenomena[4–8] but the rate-and-state friction framework has been extended to materials ranging from cardboard[9] to plastic.[10] If the frictional block remains in place, μ_s increases logarithmically with time. This is attributed to contact aging and is usually associated with contact area growing by a creep process. Applying the notion of contact rejuvenation, the models develop coupled differential equations of rate (instantaneous velocity) and state (usually associated with contact age) variables[11,12] to predict observed stick-slip and frictional creep dependencies. More recently, Rubenstein *et al.*[13] have quantitatively imaged real contact area as a function of loading versus unloading in polymethyl methacrylate (PMMA) using incident light below the Brewster angle upon a frictional interface. They observed that a finite time is required for contacting asperities to separate as normal force is reduced and termed this a "de-aging" effect. They further associated the difference in real contact area versus de-aging with a small difference in static friction coefficient (μ_s=0.44 versus μ_s=0.46).

As device dimensions are reduced in micromechanical and nanomechanical systems, the surface-to-volume ratio increases and consequently friction forces play a relatively larger role compared to inertial forces. Much attention has been focused on the relationship between the coefficient of friction in special test structures and monolayer coatings applied to such devices.[14] However, very little work has been reported that investigates loading protocol dependence.

We have developed a useful micromachined polycrystalline silicon (polysilicon) actuator[15] that can serve in applications ranging from micro-optics, microfluidics, nanopositioning, transport of heavy cargo, and nanomechanical testing. The actuator also serves as a model friction test structure, as will be described below. In our test protocol, we maintain a constant tangential force while ramping down the normal force, and look for the onset of motion, which can be measured to ± 5 nm resolution. Static friction measurements reported in a recent paper[16] indicated a comparatively large factor of three dependence of μ_s on the normal force ramp-down rate.

Because μ_s varied over such a wide range,[16] it hardly seems the most appropriate way to characterize the frictional response of the system. We postulate in this paper that a more fundamental measure of friction is provided by instantaneously dropping the normal load and then measuring the time for motion to initiate. This "instantaneous" normal force reduction is accomplished using electric-field applied force. We find that the "release time" t_r (the time for motion to initiate after the release of the normal load) varies by six

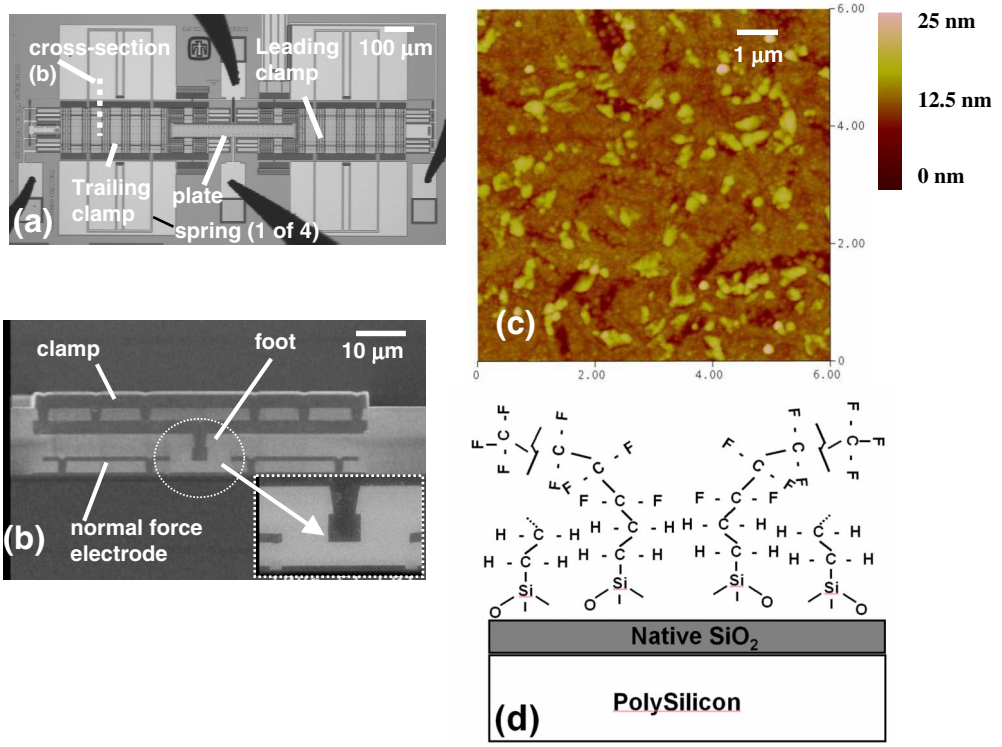

FIG. 1. (Color online) (a) Optical image of a nanotractor. Signals are applied using electrical probes. (b) SEM cross section through a clamp at the dashed line marked in (a). The inset shows the detail of the frictional counterfaces. The oxide material surrounding the polysilicon is removed by HF-acid etching prior to monolayer lubricant deposition which is described in the text. (c) AFM micrograph of a typical polysilicon surface after coating with a FOTAS organic monolayer. (d) Schematic representation of the disordered FOTAS monolayer with some chains bending out of the plane of the paper. Reprinted with permission of Journal of Microelectromechanical Systems, ©2009 IEEE.

decades, depending on the normal force hold time t_h and magnitude F_h, and on the value of the normal force after the load drop F_r (these parameters are explicitly defined below). The measurements *qualitatively* explain the previously reported ramp-down rate dependence of μ_s (Ref. 16) in terms of the de-aging concept. Applying the measured empirical release time dependence in a simple model, we *quantitatively* relate the previous μ_s measurements[16] to the present t_r measurements by introducing a "re-aging" process. The measurements of t_r also are in agreement with our previous observations that static friction decreases as hold force increases[16] and we therefore comment on the likely controlling mechanism.

II. TEST DEVICE

The nanotractor device is a friction-based stepper motor that develops a pulling force of 1 mN, travels ± 100 μm in 50-nm steps and is used to make these measurements.[15] It is pictured in Fig. 1(a) and consists of an electrostatically actuated plate and friction clamps that are attached at each end.

The geometry of the friction clamps is shown in Fig. 1(b), which is a cross section through the dashed line indicated in Fig. 1(a). An applied voltage on the normal force electrode attracts the electrically grounded clamp until the clamp foot contacts a lower grounded polysilicon layer (contact is made before the clamp has shorted to the electrode). The clamp foot makes the frictional contact and its projected area is $A_f = 600 \times 3$ μm^2. There are two feet per clamp so the total projected area per clamp is $A_c = 3600$ μm^2. With F_n calculated from a simple parallel plate law, the nominal pressure is F_n/A_c. The surface roughness of the lower and upper counterfaces is 5 nm root mean square, as measured by tapping-mode atomic force microscopy (AFM) shown in Fig. 1(c). The local asperity contact pressure can be made to approach the hardness of silicon, 11 GPa,[17] while the average asperity contact diameter D is about 10–20 nm.[15] Using previously reported contact mechanics calculations,[15] it is expected that several hundreds of asperities make contact at the apparent pressures used in this work.

The nanotractor is fabricated from five structural layers of polycrystalline silicon (polysilicon) using the SUMMiT V™ process.[18]. As friction is an interfacial property, it can be greatly influenced by the presence of a monolayer.[19] Here, a vapor-deposited 1.2-nm-thick monolayer lubricant (tridecafluoro-1,1,2,2-tetrahydrodecyltris(dimethylamino) silane, $CF_3C_5F_{10}C_2H_4Si[N(CH_3)_2]_3$, FOTAS) (Ref. 20) conformally coats the device to reduce the junction shear strength, thereby minimizing friction.[21] The resulting surface is hydrophobic with a water contact angle of 106°; thus minimal capillary condensation due to ambient moisture is expected. The eight-carbon chains are relatively short and the fluorocarbon radius is larger than the head group attachment. Van der Waals forces between the tail groups are too small to

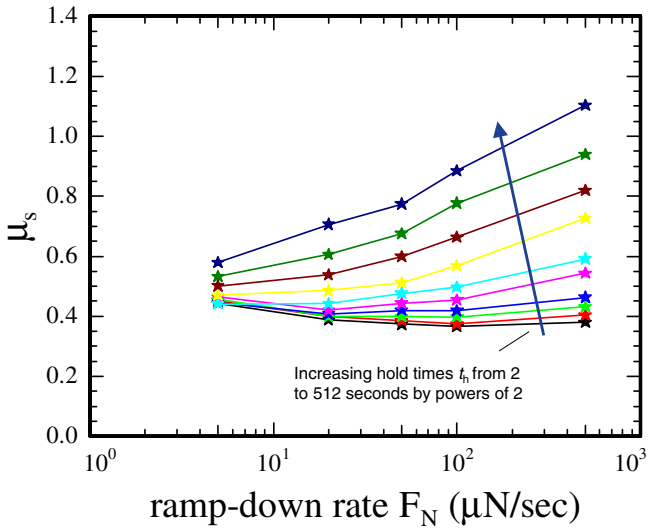

FIG. 2. (Color online) Coefficient of static friction as a function of ramp-down rate for ten different hold times all taken at the same hold force, Fh=1700 μN. For all ramp-down rates, static friction aging is evident. Reprinted with permission of Journal of Microelectromechanical Systems, ©2009 IEEE.

achieve local alignment, and instead the chains are likely disordered,[22] as represented in Fig. 1(d). [Compared to our first nanotractor paper,[15] the nanotractor feet studied more recently[16] and in the present work are nominally flat. This is due to a change in how the feet are fabricated. They were previously formed by filling a partially plasma-etched deposited sacrificial oxide layer with polysilicon. This etch left a convex surface behind as can be seen in Fig. 4(c) of the first nanotractor paper.[15] In the more recent[16] and the present work, the feet are placed on top of that sacrificial oxide layer. The nominal pressure for the same applied force is now approximately thirty times less. For the present work, an estimate of real to apparent contact area ratio of $\sim 3 \times 10^{-5}$ at an apparent pressure of 0.5 MPa can be made [based on Fig. 16(a) (Ref. 15)]. In Greenwood-Williamson contact mechanics of rough surfaces,[3] average asperity pressure is only weakly dependent on apparent pressure and therefore the estimated fraction of contacting asperities under loads approaching the hardness of silicon remains 0.6.]

As shown in Fig. 2, the static friction coefficient measured depends strongly on the normal ramp-down rate. As described in detail in the companion paper,[16] which summarized repeatable results from four different SUMMiT V™ lots and a total of eight different monolayer coating runs, this data was taken in the following way. First, the nanotractor was walked out to a position $x_o=30$ μm using pattern matching combined with a positioning algorithm (to ± 50 nm precision as limited by the nanotractor step size), thereby setting the applied tangential force F_t to 450 μN (the stiffness of the suspension springs on the nanotractor is 15 N/m). Then, the normal force was set to a hold force value of $F_h=1700$ μN by applying electrostatic voltage to the leading clamp (the clamp further removed from the zero position). After a hold time t_h as indicated in Fig. 2, the normal force was ramped down at a constant ramp-down rate. $\dot{F}_n$ to measure the static friction coefficient. The static friction coefficient value was defined by $\mu_s=F_t/F_n$, with F_n set by the first perceptible position change of the nanotractor, which was measured by optical microscopy to ± 5 nanometer accuracy using subpixel interpolation. If there were no aging of the interface during the hold and no dependence on ramp-down rate, we would expect no difference in the measured μ_s values.

Furthermore, as hold force F_h was increased, the static friction coefficient decreased.[16] This appears to be contrary to expectations from other work that has examined aging effects.[10,23] That is, at higher normal loads in rock and PMMA, creep at the heavily loaded contacts increases the contact area of the bulk material. Therefore, from those material studies, it would be expected that the static friction coefficient would increase with increasing hold load. However, it is in agreement with a different interpretation,[24] which is that the rate of static friction aging increases with the shear to normal hold force ratio (F_t/F_h) as long as the block does not move during the hold. By examining the data in the companion paper (see discussion section of the recent work[16]), we arrived at a similar conclusion. [The ramp-down rate is controlled digitally and the normal force step size is established by the camera video rate of 15 frames per second. The ramp down begins at the hold force F_h. For a ramp-down rate of 1 μN/s, the normal force increment is 0.07 μN per frame, while for a ramp-down rate of 20 μN/s the normal force increment is 35 μN/frame (2% of F_h). The normal force depends on V_c^2, where V_c is the applied clamp voltage.]

In this work, we wish to understand the origin of two important observations[16] in greater detail. They are listed in Table I and include the normal-force ramp-down dependence of μ_s as in Fig. 2 and the *decrease* in the aging rate of μ_s at larger F_h values.

TABLE I. Previous and current correlating observations.

	Previous observation (Ref. 16)	Correlating observation (this work)
1	μ_s depends on hold time t_h and normal force ramp-down rate $\dot{F}_n$ (Fig. 2 in this work)	Time until block moves (t_r) after reducing hold force is much greater than inertial response time and depends on t_h and force on clamp after release (F_r)
2	Rate of static friction coefficient aging decreases as F_h increases [Fig. 8 (Ref. 16)]	t_r decreases as F_h increases

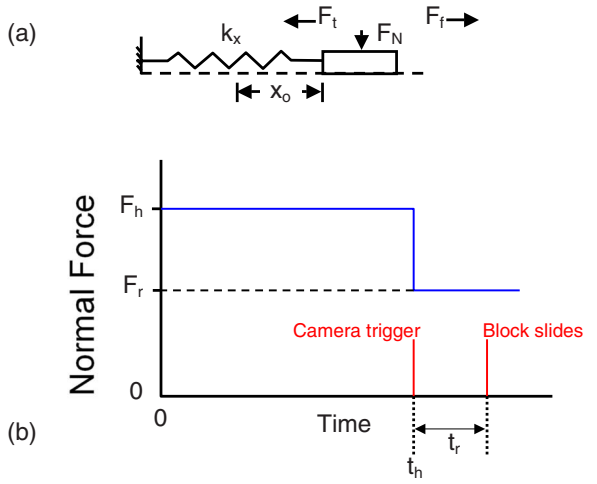

FIG. 3. (Color online) (a) Equivalent mass and spring representation of a nanotractor. F_n is the electrostatically applied normal force, F_t is the tangential force, F_f is the friction force, k_x is the spring constant of the suspension springs, and x_0 is the extension of the spring beyond its rest length. (b) A timing diagram showing the triggering of the high-speed camera simultaneously with the dropping of the normal force after holding for a time t_h from the hold force, F_h, to the release force, F_r. The release time, t_r, is then measured as the time to first motion after the camera is triggered.

III. MEASUREMENT

Given the large range of normal force ramp-down rates explored in Fig. 2, it appears that there is no sufficiently high ramp-down rate at which the μ_s value saturates. Rather, the data is always a function of hold time t_h, and ramp-down rate $\dot{F}_n$. We postulate that even if the normal force were lowered instantaneously after the hold, the time for the block to begin moving, the release time t_r, would be greater than the inertial response time. Though this procedure sacrifices any attempt at measuring μ_s, we shall find that we can relate the measured t_r to the μ_s trends presented in Fig. 2. We explore previous observation 1 in Table I by measuring the effect of hold time t_h and release force F_r (defined in the next paragraph) on release time t_r and we investigate previous observation 2 in Table I by measuring the change in t_r as F_h is varied.

To measure t_r, the nanotractor was moved to an initial position $x_o=30$ μm and held there for a prescribed amount of time t_h and at a prescribed normal hold force F_h. We do not include the small corrections in F_h from adhesion (~ 5 μN) or from the small out-of-plane restoring force from the suspension springs (~ 0.3 μN) (Ref. 25) in the normal force calculation. The tangential force F_t experienced during the hold was again set by the stiffness of the suspension spring, and was $k_x x_o=450$ μN, where $k_x=15$ N/m. The normal force was then dropped to a release force, F_r, by decreasing the clamp voltage. Note that for the same value of F_h, lower values of F_r indicate larger normal force drops, corresponding to a larger driving force, and hence were expected to correlate with shorter release times. Figure 3(b) shows a timing diagram of this operation. Due to the capacitance of the device and the slew rate of the amplifier (Tegam Model 2350) driven by a digital to analog card (National Instruments PCI-6733), the voltage was reduced from F_h to F_r in approximately 1 μs. This normal force reduction time was verified with an oscilloscope.

The release time, t_r, was captured with a high speed camera (Phantom V5) that was triggered to start recording at the same time as the drop in normal force from F_h to F_r. The camera was attached to a Mitutoyo FS70 microscope (20× objective, NA=0.42) on a Signatone probe station and captured images as fast as 10 000 frames per second with a 90 μs exposure time. For some time after the drop in force, the nanotractor showed no detectable motion, and then abruptly jumped to a final rest position. The release time could be determined to approximately 100 μs resolution from the recorded video for jumps of 1 μm or greater. Typical jump sizes were tens of microns and the 1 μm lower bound limit on detectable jump size was set by our ability to detect a change in motion visually by reviewing the frames but without saving data to disk. While measurements of jump sizes smaller than 1 μm could be made from captured high-speed video, identifying these would have required saving very large image data sets (2 GB) for postprocessing and would have greatly increased the measurement time. With this technique the dependence of t_r on the parameters t_h, F_h, and F_r was determined. All data was taken in laboratory air at room temperature with a relative humidity of approximately 30%, similar to the measurements in the companion paper.[16]

Ignoring for the moment any dependence of t_r on t_h, if a minimum distance of $x_{\min}=1$ μm could be detected and if the resisting tangential force was dropped from a value above $k_x x_o$ to a value $\mu_d F_r$ significantly below $k_x x_o$, an expected inertial release time is

$$t_i \approx \sqrt{\frac{2mx_{\min}}{k_x x_o - \mu_d F_r}}, \tag{1}$$

where u_d is the coefficient of dynamic friction (where $u_d=0.2$). Given the spring constant ($k_x=15$ N/m) and the mass of the nanotractor ($m=2.25\times10^{-9}$ kg), t_r would equal an inertial response time of about $t_i=5$ μs if F_H were dropped to $F_r=955$ μN. Consideration of the experimental range of F_r values in Sec. IV below implies that all the release times would occur in the first camera frame (100 μs) and that our experiment would not have resolved any dependence on F_h or F_r.

IV. RESULTS

We first conducted scoping experiments on four devices that revealed the trends and aided in selecting parameter ranges. Our complete data set from a final device consists of 120 measurements with a range of t_h from 16 to 512 s, F_h from 1560.55 to 2150.55 μN, and F_r from 663.5 to 955.8 μN (see Table II). The measured release times over this range of parameters varied from less than 100 μs to almost 50 s. Figure 4 shows three sample plots from the data sets, each plotting release time as a function of one of the three parameters (with two lines on each plot to show varia-

TABLE II. Experimental parameters used to take data in Fig. 4.

Parameter	Values
t_h (s)	16, 32, 64, 128, 256, 512
F_r (μN)	663.75, 755.2, 852.55, 955.8
F_h (μN)	1560.55, 1699.2, 1843.75, 1994.2, 2150.55

tion with respect to the other two parameters). From these plots it is seen that t_r depends on each of the three parameters through some function

$$t_r = f(t_h, F_h, F_r). \tag{2}$$

The appropriate form for this function can be determined by examining the interdependencies of the various parameters.

The first observation from these high-speed camera measurements is that for all fixed values of F_h and F_r, an increase in t_h leads to an increase in t_r. Thus, if we consider t_r as a measure of de-aging, aging is occurring between the two contacting surfaces (assuming de-aging is directly related to aging[13]). Figure 4(a) contains a log-log plot showing the increase in t_r with t_h. The two data sets were taken for different pairs of the parameters F_h and F_r. The linear behavior suggests a power-law dependence of release time on hold time of the form

$$t_r \propto t_h^n. \tag{3}$$

The red line through both sets of data is plotted with the same value of the exponent n and was determined by fitting all of the data to a final functional form in which the only dependence on hold time is through the above power law. This demonstrates that the scaling of t_r with t_h is independent of both F_h and F_r.

A supporting demonstration that aging occurs is shown by resetting the nanotractor after a hold. By moving the block by as little as 50 nm (a single step of the nanotractor) after aging but before dropping to F_r, the release-time enhancement due to aging is entirely removed. For example, with t_h=32 s, F_h=1699.2 μN, and F_r=955.8 μN, the measured release time is 27 500 μs when dropping right from F_h to F_r, while a release time of less than 100 μs is measured when taking a single step after aging but before release. This rejuvenation of the contacting surfaces, similar to our observations of rejuvenation after 200 nm of motion in static friction measurements,[16] conforms with observations from both rate-state friction and unloading hysteresis measurements.[10,13]

The dependence of t_r on F_r can also be measured by fixing F_h and t_h and varying F_r. Figure 4(b) shows a semilog plot of t_r as a function of F_r. The two data sets plotted are taken for different pairs of the parameters F_h and t_h. The

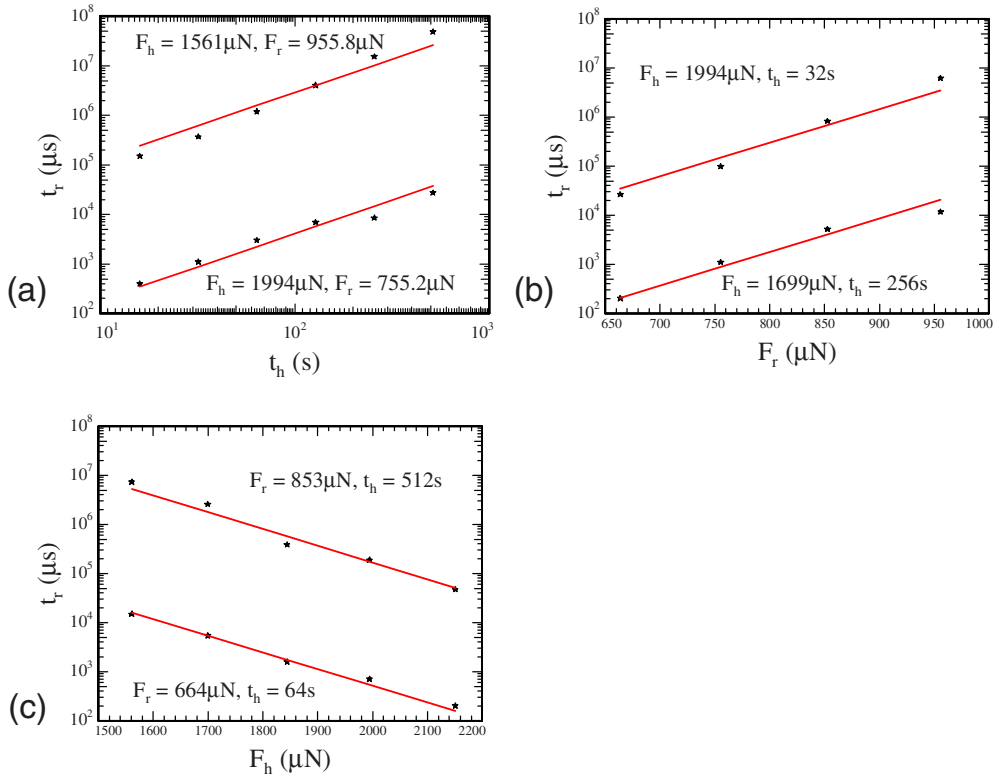

FIG. 4. (Color online) Plots showing the various dependencies of the release time. Experimental parameters are summarized in Table II. (a) A log-log plot showing how t_r varies with t_h for two different sets of F_h and F_r. The red lines are power-law fits with the same exponent for each. (b) A log-linear plot showing how t_r depends on F_h for two different sets of F_r and t_h. The red lines are exponential fits with the same constant for each. (c) A log-linear plot showing how t_r depends on F_r for two different sets of F_h and t_h. The red lines are exponential fits with the same constant for each.

TABLE III. Best fit parameters for Figs. 4, 5, 6(b), 7, and 8.

Parameter	Value
a	332.97 ms
n	1.2866
b_1	0.01486 μN^{-1}
b_2	−0.007358 μN^{-1}
b_3	−0.0036 μN^{-1}

linear behavior reveals that t_r increases exponentially with F_r with the form

$$t_r \propto e^{F_r b_1}. \quad (4)$$

The red line through both sets of data is plotted with the same value of coefficient b_1 and was determined by fitting all of the data to a final functional form in which the above exponential form is the only dependence on release force. Thus the scaling of t_r with F_r is independent of both F_h and t_h.

Finally, the dependence of release time on hold force can be determined by fixing F_r and t_h and varying F_h. Figure 4(c) shows a semilog plot of t_r as a function of F_h. The two data sets plotted are taken for different pairs of the parameters F_r and t_r. The linear behavior reveals that t_r decreases exponentially with F_h with the form

$$t_r \propto e^{F_h b_2}. \quad (5)$$

The red line through both sets of data is plotted with the same value of coefficient b_2 and was determined by fitting all of the data to a final functional form in which the above exponential form is the only dependence on hold force. Thus the scaling of t_r with F_h is independent of both F_r and t_h. The observation that the slope in Fig. 4(c) is negative is in qualitative agreement with observation 2 on the left side of Table I.

The full functional form is simply a combination of the three dependencies and can be written as

$$t_r/t_o = (a/t_o)(t_h/t_o)^n e^{F_r b_1 + F_h b_2}, \quad (6)$$

where $t_o = 1$ s. Taking the natural log of both sides yields

$$\ln(t_r/t_o) = \ln(a/t_o) + n \ln(t_h) + b_1 F_r + b_2 F_h. \quad (7)$$

Using this form, the data can be approximated by a least-squares fit with the four adjustable parameters, a, n, b_1, and b_2. The best fit parameters are shown in Table III and were also used to draw the red lines in Fig. 4. Figure 5 displays a plot of fit times versus the measured release times for all 120 points and demonstrates a good fit over the entire range of the data. The inset in Fig. 5 shows that the maximum error between the fit and the data is a factor of 5 over the six decades of data.

V. DISCUSSION

Our results show that release time t_r in this interfacial system depends on both the full force history through the hold time t_h, the hold force F_h, and the release force F_r. Qualitatively it is clear that the ramp-down dependence of μ_s in Fig. 2 correlates with t_r. That is, for high ramp-down rates, F_n reaches a lower value before a slip event because it takes a certain amount of time before the interface releases, resulting in a higher value of μ_s. Our goal then is to develop a quantitative relationship between μ_s and t_r. To accomplish this, we first discuss our measurements in light of recent work[13] to gain perspective on the present experiments and to aide in establishing a framework.

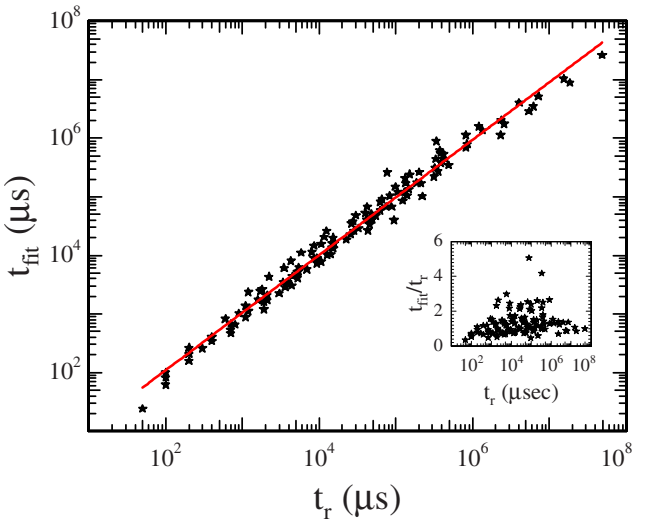

FIG. 5. (Color online) Goodness of model fit shown by log-log plot of predicted release time versus of true release time for every set of t_h, F_h, and F_r. The red line is a linear fit. The inset shows that over almost 6 orders of magnitude the fit is within a factor of 5 of the data.

Rubinstein *et al.*[13] use an elegant direct imaging technique to study the difference in real contact area while loading and unloading. While Rubinstein *et al.* report on the importance of de-aging, i.e., the "time-dependent decrease in *real contact area* at fixed load after a certain amount of unloading has occurred," the primary effect discussed in their paper is an elastoplastic one. They are able, however, to decouple these effects, as explained next. In their experiment, applying normal force only, they load and unload a PMMA block and quantify the difference in real contact area. During unloading, the contact area is noticeably larger than during loading; that is, there is substantial hysteresis in this experiment. The measured curves are repeatable even though the PMMA block is ostensibly in the same position during each loading cycle. If this result were due to plastic deformation of the same set of asperities, reloading would occur along the previous unloading line, but this is not observed. After carefully investigating their data, they arrive at the conclusion that during each loading cycle, different sets of asperities come into contact due to a Poisson extension which is substantial because PMMA is an elastically soft material ($E \sim 4$ GPa). The loading cycles are repeatable because each loading cycle is an elastoplastic curve for essentially virgin asperities. They also measure a small and noisy difference in μ_s by applying tangential force during the loading and unloading portions of the cycle (0.44 upon loading and 0.46 upon unloading).

In a typical loading cycle, Rubinstein *et al.* load and immediately unload at a fixed rate. To decouple the effect of de-aging from elastoplasticity, they hold the force at its maximum value for some time before unloading [see Fig. 5(a) in Rubinstein *et al.*[13]]. They then observe a growth in contact area, which they ascribe to contact aging. Upon unloading, the real contact area is substantially larger than when unloading without aging. After a certain amount of unloading, they hold the force at a fixed value and then observe that the real contact area shrinks with time, i.e., contact de-aging.

In the present paper, measurements focus on the effects of unloading protocol on (i) static friction (Fig. 2) and on release time (Figs. 4 and 5). As seen in Fig. 2, μ_s depends strongly on both t_h and $\dot{F}_n$. The 200% variation in μ_s depending on unloading protocol is much greater than Rubinstein's 4% difference in μ_s on loading versus unloading and it can be said that a real-time imaging method is not necessary in our experiments in order to observe a significant effect of loading protocol on friction.

Also in our experiments, Poisson extension very unlikely plays a confounding role because of the much higher modulus. Assuming free slip of the interface, the maximum contraction is

$$\Delta = \nu \frac{F_h/A_c}{2E} L_{block}, \tag{8}$$

where the factor of 2 assumes the center of the block remains stationary. This extension will increase linearly from the center of the block. With $L_{block}=600$ μm, $\nu=0.22$, $F_h=1700$ μN, $E=164$ GPa,[26] and $A_c=3600$ μm^2, $\Delta=0.2$ nm. This is much smaller than the expected diameter of the contacting asperities, which is about 10–20 nm.[15] If we redefine de-aging to mean "the time-dependent reduction in *friction* (rather than real contact area) at fixed load after a certain amount of unloading has occurred," we can qualitatively state that the measurements in Fig. 2 reflect the aging (through t_h) and ramp-down rate (through $\dot{F}_n$) dependencies of de-aging. The de-aging definition used here redirects attention to the mechanical response of the system and is necessary because the decrease in μ_s may not be due to a change in the real contact area but rather to a molecular reconfiguration at the contacting asperities.[27]

The measurement of t_r is the focus of the experimental section. After having aged the interface for time t_h under various hold loads F_h, t_r (as a function of F_r) is the time needed to de-age the interface to the degree that it is weak enough to slide. Thus t_r is not a direct measure of de-aging but rather the time that it takes the interface to reach a certain "weak" state by a de-aging process after it has been aged to a "strong" state. Rubinstein *et al.* directly show that de-aging takes place but they do not investigate its dependencies on loading protocol. Our measurements represent a systematic study (in which Poisson extension is likely not a confounding factor) of the effects of aging on the time that it takes to de-age the interface to a certain state.

The measurements show that the parameters t_h, F_h, and F_r control t_r in a systematic fashion over six decades. How much further might this range extend? At the low end we can speculate that the range of t_r in Fig. 5 may be as short as the time it takes for molecular bonds to form. Experimentally, this is limited by the time it takes to drop the load, which is currently about 1 μs. A more fundamental lower limit is that the inertial response time of the system is on the order of 5 μs and the effect of interface strength on t_r becomes difficult to differentiate once t_r is on this order. On the high end, Eq. (7) will eventually not apply because aging processes compete with de-aging processes. Therefore, we expect that for some sufficiently high F_r value, t_r will approach infinity. We shall call the release force at which de-aging begins $F_{\text{de-age}}$.

In view of this discussion, we are in position to better understand observation 1 by searching for a quantitative relationship between t_r and $\mu_s(\dot{F}_n)$ that can be physically motivated. We begin by considering the integrated fraction of release time spent at each normal force (starting from F_h and ramping down with a rate $\dot{F}_n$), and assume that a jump will occur when this fraction equals one, determining the time t_{jmp} until a jump. Using Eq. (6) (where t_o has been dropped to simplify the expression)

$$1 = \int_0^{t_{jmp}} \frac{dt}{a t_h^n e^{(F_h - \dot{F}_n t) b_1 + F_h b_2}}. \tag{9}$$

The integrand can be thought of as the fractional amount of de-aging. Here we assign $F_r = F_h - \dot{F}_n t$ to capture the normal force ramp down of Fig. 2. Strictly, the lower integral limit should be $t_{\text{de-age}}$, which represents the time associated with $F_{\text{de-age}}$ when de-aging begins. However, the relative value of the integrand at high normal forces (small t) is very small; nearly all of the contribution to the integral occurs near the end of the jump time. Solving for the jump time, we obtain

$$t_{jmp} = \frac{\ln\{1 + a b_1 \dot{F}_n t_h^n \exp[F_h(b_1 + b_2)]\}}{b_1 \dot{F}_n}. \tag{10}$$

The normal force at which the μ_s value is observed in Fig. 2 can then be written as

$$F_{jmp} = F_h - \dot{F}_n t_{jmp}. \tag{11}$$

Given a tangential force F_t, the coefficient of static friction can be written as

$$\mu_s = \frac{F_T}{F_{jmp}}. \tag{12}$$

Figure 6(a) shows the model of μ_s as a function of ramp rate for four different hold times using the parameter values from Table II. While the model qualitatively shows that increasing ramp rate results in a higher value of μ_s, it significantly underpredicts the data.

In writing Eq. (9), we replaced F_r in Eq. (6) with $F_h - \dot{F}_n t$, meaning that fractional de-aging was sustained equally well for past as well as recent times. A simple weighting function that accounts for the possibility that past de-aging is less effective than recent de-aging can be introduced with a parameter b_3. Accordingly,

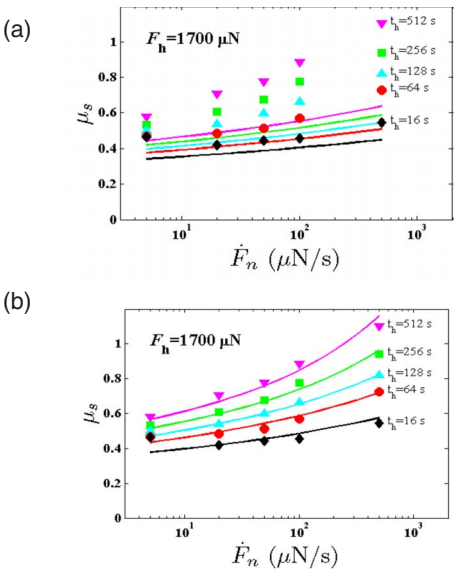

FIG. 6. (Color online) Comparison of data to model. Symbols are selected data from Fig. 2 with corresponding hold times and lines show model. (a) Model based on the assumption that a partially de-aged interface remains de-aged [Eqs. (10)–(12)] qualitatively shows the correct trend but significantly underpredicts the data. (b) Model weighting the recent de-aging history by allowing re-aging during the ramp down [Eqs. (11), (12), and (15)].

$$1 = \int_0^{t_{jmp}} \frac{dt}{a t_h^n e^{-\dot{F}_n t(b_1+b_3)+F_h(b_1+b_2+b_3)}}. \tag{13}$$

Allowing b_3 as a free parameter improves the fit with respect to Fig. 6(a) (with $b_3=+0.004/\mu$N)—the model predictions for different t_h values are increased but are more closely spaced with respect to t_h than the data. If b_3 modifies only F_h in Eq. (8), the fit is further improved (with $b_3=+0.0021/\mu$N), but the model fit remains tighter than the data. These forms are discounted because they mean that the fractional de-aging would be influenced by F_h through b_3 (which is associated with de-aging) after ramp-down begins. Also, with b_3 positive, they predict that the fractional de-aging is larger when there is a finite ramp-down rate than when there is an instantaneous ramp down. However, if b_3 modifies only $\dot{F}_n t$, we write

$$1 = \int_0^{t_{jmp}} \frac{dt}{a t_h^n e^{-\dot{F}_n t(b_1+b_3)+F_h(b_1+b_2)}}. \tag{14}$$

This form means that once the ramp-down begins, fractional de-aging depends only on the ramp-down rate $\dot{F}_n$. In other words, F_h and t_h set the interface initial conditions from which the contacts de-age and $\dot{F}_n$ establishes the rate at which fractional de-aging occurs. The result for t_{jmp} becomes

$$t_{jmp} = \frac{\ln\{1 + a(b_1+b_3)\dot{F}_n t_h^n \exp[F_h(b_1+b_2)]\}}{(b_1+b_3)\dot{F}_n}. \tag{15}$$

With only b_3 as a free parameter, the good fit to the data now found is seen in Fig. 6(b). Note that $b_3=-0.0036/\mu$N (as reported in Table III) is negative but that the quantity (b_1+b_3) is positive, consistent with the view that recent fractional de-aging is more effective than past fractional de-aging. That is, contacts that have been de-aged at some $F_r > F_{jmp}$ begin to "re-age." Mathematically, the denominator in the fractional de-aging quantity increases because $(b_1+b_3)<b_1$, increasing t_{jmp}, thereby decreasing F_{jmp} and finally increasing μ_s. In detail, the model describes the data reasonably well for t_h=512, 256, 128, and 64 s but not as well for t_h=16 s. Specifically, at t_h=16 s and $\dot{F}_n$=5 μN/s, the measured data point for μ_s increases noticeably relative to its lowest value. This is because the ramp-down time is much longer than the hold time so that the interface begins aging during the ramp down (before the normal force reaches $F_{\text{de-age}}$). This effect is not accounted for because the model assumes that once a ramp-down begins, the dependence on F_h is erased.

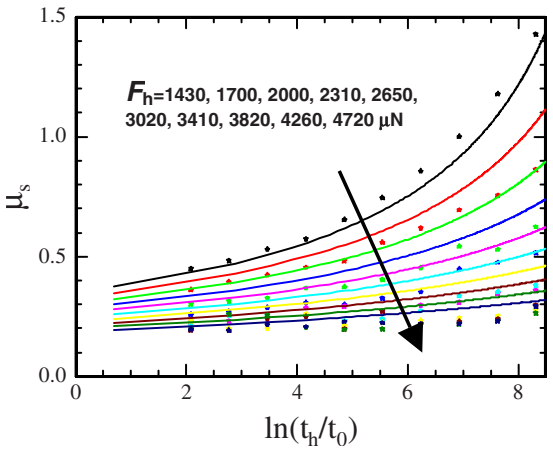

FIG. 7. (Color online) Comparison of Eq. (16) with the experimental data from Fig. 8(b) of Ref. 16.

With the good agreement, we can seek to generalize the applicability of Eqs. (11), (12), and (15). Figure 6(b) shows that they fit the data well but this is only at only one value of F_h. Combining the equations yields

$$\mu_s = \frac{F_T}{F_{jmp}} = \frac{F_T}{F_h - \dot{F}_n t_{jmp}} = \frac{F_T(b_1+b_3)}{F_h(b_1+b_3) - \ln\{1 + a(b_1+b_3)\dot{F}_n t_h^n \exp[F_h(b_1+b_3)]\}}. \tag{16}$$

As previously detailed [Figs. 8(a)–8(c) (Ref. 16) and the adjoining discussion], μ_s depends strongly on F_h, and the logarithmic rate of aging, β, decreases with increasing F_h. Similarly, release time in this work release time t_r also decreases with increasing F_h.

In Fig. 7, μ_s versus $\ln(t_h)$ is plotted for different values of F_h using Eq. (16), with $\dot{F}_n$=30 μN/s as used in the experiment.[16] The experimental data with the same F_h values are also shown [Fig. 8(b) (Ref. 16)]. We maintain the parameters of Table III and in particular keep the re-aging parameter b_3. For the lowest F_h value, the agreement between Eq.

(16) and the data is very good. As F_h increases, the trend remains, although the data indicates that the μ_s values drop somewhat more quickly with F_h than the model predicts. Recalling that b_3 is an adjustable parameter in Table III, we explored different values to look for a better fit but find that $b_3=-0.0036$ remains a good choice in Figs. 6(b) and 7 to match the experimental data. The greatest model sensitivity to b_3 is revealed in Fig. 7 at the lowest value of F_h and this can be understood because the logarithmic aging rate is greatest here.

It is common in rate-and-state friction laws to assume that the logarithmic aging rate β is a constant and its value was taken by making a linear fit[16] to the data in Fig. 7 over the range $4<\ln(t_h)<8$. An analytic expression for β can then be found by linearizing about the middle of the hold-time range $[\ln(t_h)=6]$. The second term inside the natural log in Eq. (16) is much greater than 1 for all experimental values and therefore dominates. Then

$$\beta = \left.\frac{\partial \mu_s}{\partial \ln(t_h)}\right|_{\dot{F}_n,F_h} = \frac{F_T n(b_1+b_3)}{[F_h(b_1+b_3)-\ln\{a(b_1+b_3)\dot{F}_n t_h^n \exp[F_h(b_1+b_3)]\}-n\ln(t_h)]^2}. \tag{17}$$

We plot this expression in Fig. 8 using $\ln(t_h)=6$, the parameters of Table III and $\dot{F}_n=30$ μN/s in order to compare with the data [Fig. 8(c) (Ref. 16)]. We see that the fit (green solid line) in Fig. 8 is very good. For comparison, we also plot Eq. (17) in Fig. 8 using a value of $b_3=0$ (the blue dashed line). Because β is most sensitive to F_h at low values of F_h, the best comparison is in that realm, and it is again seen that $b_3=-0.0036$ fits the data significantly better than $b_3=0$.

Therefore, we broaden our assertion that release time t_r is the underlying fundamental parameter that controls the measured μ_s values in all the previous experimental results on static friction coefficient.[16] Furthermore, because a value of b_3 that is negative and distinctly different from zero best fits the data taken in different ways, the concept of re-aging is more strongly supported.

Having quantitatively related t_r to μ_s by introducing the concept of re-aging, we now wish to better understand observation 2 in Table I. Both μ_s and t_r are reduced by increasing F_h. The static friction coefficient data (Fig. 2) is one result from an extensive study on this interface,[16] while t_r, as reported here, is a more fundamental measurement quantity.

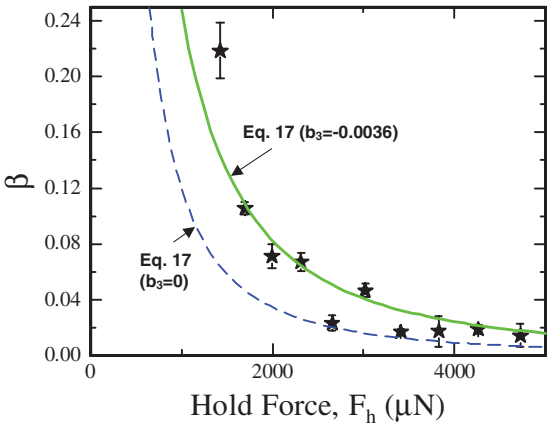

FIG. 8. (Color online) Comparison of Fig. 17 with the experimental data from Fig. 8(c) of Ref. 16.

To probe more deeply, we must ask why t_r exhibits the dependencies with respect to F_h we have observed. We can suggest two mechanisms for the aging behavior. The first is that the contact area increases with time due to material creep, while the second is that entanglement of disordered monolayer chains themselves, similar to the interpretation of Yoshizawa and Israelachvili.[27]

Future experiments could resolve which mechanism is more likely operating. If the first prevails, real contact imaging (although more difficult with such small contacts) would show an increase with time. Also, in rate-and-state theory, the state variable theta (the effective age of the contact, referred to as "state") would continue to increase for a rough on smooth interface even if the surfaces experienced relative motion. If the second mechanism governs, under static conditions the real contact area would remain the same with time while contact memory would be erased for a rough on smooth interface for relative motion greater than a typical chain entanglement length. In an AFM experiment, *xy* drift less than 1 nm over many minutes would be required in order to observe aging effects. Such data could link the length scale from a single nanometer contact to hundreds of multiscale contacts in the micromachining situation.

Based on experiments performed for rock on rock, Linker and Dieterich[23] proposed a law for the time-dependent change in state as a result of a sudden change in normal stress. While maintaining a constant velocity (to ensure renewal of state), the steady-state change in friction was not immediately reached upon an increase in normal stress. Therefore, state initially decreased upon a sudden increase in normal stress because of the time needed for creep processes to attain the larger associated asperity contact area. Eventually, however, the coefficient of friction always reached a constant value independent of the stress change. Likewise, state temporarily increased upon a normal stress reduction. Mechanistically, this was interpreted as an underaging (overaging) effect for normal stress increase (decrease), reflecting material creep. This is different from our results where we see after long hold times that both static friction coefficient[16]

and release time decrease with increasing hold force. That is, after a hold at high F_h, creep would increase the asperity area if this model[23] applies. Then with a rapid normal force reduction, the expected μ_s would be higher instead of the lower value we measured.[16]

Hence it appears more likely that the molecular bonding mechanism operates, and manifests in both the μ_s measurements and the t_r measurements. This is further supported by the observation that silicon does not exhibit perceptible creep in room-temperature indentation experiments.[28] Also, in a Hertz contact, large sub-surface shear stresses exist, and therefore increasing F_n increases the shear stress in the bulk polysilicon material. Because of the large fraction of plastically loaded contacts (a value of 0.6 was estimated[15]), creep could ensue, leading to an increase in contact area and hence increasing μ_s. Yet we see a decrease rather than an increase in μ_s as F_h increases. The observations of Bureau *et al.*[24] that increased shear increases aging, when viewed as scaling with F_t/F_h are consistent with our static friction and release time results. However, in this micromachined interface, increasing F_t/F_h may increase the molecular bonding rate rather than the bulk material rate of creep.

If intercalation of the molecular chains is the primary aging mechanism, we must reexamine whether elastic Poisson contraction plays a role in the experiments. That is, even though the estimated maximum contraction of 0.2 nm is small, it is somewhat larger than the length of molecular bonds. As normal force is first applied, Poisson extension will occur to the degree that the interface can slip. During the hold, any slip will compete with interface aging and thus further change in maximum extension can be expected to be smaller than 0.2 nm. When normal force is released, any elastic component of interface slip due to Poisson contraction will occur quickly compared to the release times measured in these experiments and therefore is not expected to contribute to the measured time dependencies. Hence, if Poisson contraction is playing a role, the measured values of t_r would only increase. Because the t_r values are already so large, and because closer to its center the block can only slip less, it seems unlikely that Poisson contraction has a significant effect on t_r.

How can the proposed re-aging mechanism occur while the force continues to ramp down? We contemplate this question by considering two extremes as to how release occurs after an instantaneous ramp down. In the first, when normal force is reduced, a certain fraction of asperities comes out of contact. The remaining loaded asperities can no longer sustain the shear force and therefore contacts are rapidly broken until release. The detail of how this occurs is an interesting subject, likely involving sonic crack propagation.[29] In the second, as force is removed, all asperities remain in contact. Those asperities that, from elastic theory, would have been separated, remain in contact by stretching the monolayer chains across the interface.

In this first extreme, re-aging could occur during a slow normal force ramp-down process because the normal force attains a low value at which the rate of aging has been observed to be higher. However, the extra amount of time that asperities remain in contact is small compared to t_h and an exponential rather than a power-law aging law in this regime fits the data. Thus, re-aging in this context seems unlikely. In the second extreme, re-aging of stretched monolayer molecules could occur. Such molecules have been prealigned into energetically favorable states during the hold. Some of the bonds formed will remain intact, making it easier for bonds that have been broken to reform. It is plausible that bond reforming under tension would occur with a different dependence (i.e., exponential) than the original bond forming under compression (i.e., power law). Most likely, the actual interface state lies somewhere in between these extremes and the re-aging stems from a component due to the second extreme.

VI. SUMMARY AND CONCLUSIONS

In this work, we have investigated the origin of a strong dependence of static friction coefficient on normal-force ramp-down rate as previously reported.[16] There, μ_s varied by nearly 200% depending on measurement protocol. Here we find that interface de-aging is the underlying mechanism that controls those static friction coefficients. The quantity release time t_r is a more fundamental measure of interface strength than static friction. In this work, it is an indirect measure of de-aging—it is the time for the interface to reach a certain state after it has been subjected to a certain loading protocol. However, unlike in Rubinstein *et al.*,[13] de-aging is likely not confounded with a Poisson effect because of the high modulus silicon material. Also, a real-time imaging measurement is not needed; rather friction can unambiguously associated with de-aging. The quantity t_r exhibits strong dependencies qualitatively similar to the static friction[16] measurements and varies over six decades according to the loading protocol. By introducing the concept of fractional de-aging and re-aging as the force is ramped down, it was shown that μ_s can be quantitatively related to t_r. The effects are most likely due to time-dependent molecular bonding effects, which are enhanced by shear. It would be of interest to examine the proposed re-aging process in more depth by measuring dependencies of t_r on the unloading protocol. For example, one could instantaneously change F_r before motion is detected to test if t_r is the superposition of controlled fractional release times.

The effects of temperature, monolayer chain length and coverage, would all be of interest in subsequent studies. Wear is an important problem and can perhaps be solved with alcohol vapor-phase coatings.[30] What protocol-dependent effects will be observed if these tests are performed while exposed to an undersaturated vapor? Wear can also be addressed by applying hard coatings. However, in this case we might expect that adsorbed monolayers (i.e., adventitious hydrocarbons) will affect the results. The ultimate goal in this work is to achieve an understanding of what monolayers are most appropriate in achieving reproducible performance for friction-based microactuator and nanoactuator, which are potentially very useful in positioning, microrobotics, and optical and medical applications. Here we have shown that release time is an important quantity needed to understand static friction values.

ACKNOWLEDGMENTS

The authors acknowledge the staff at the Microelectronics Laboratory for their reliable fabrication and coating of nanotractor actuators. Sandia is a multiprogram laboratory operated by Sandia Corporation, a Lockheed-Martin Co., for the United States Department of Energy under Contract No. DE-AC04-94AL85000.

*Present address: Micro-Systems and Micro-Fluidics Laboratory, General Electric Corp., Niskayuna, New York 12309, USA.

†Present address: Mechanical Engineering Dept., Carnegie Mellon University, Pittsburgh, PA 15237, USA.

[1] D. Dowson, *History of Tribology* (Longman, London, New York, 1979).

[2] F. P. Bowden and D. Tabor, *Friction and Lubrication of Solids: Part I* (Oxford University Press, Oxford, UK, 1950).

[3] J. A. Greenwood and J. B. P. Williamson, Proc. R. Soc. London, Ser. A **295**, 300 (1966).

[4] J. H. Dieterich, J. Geophys. Res. **77**, 3690 (1972).

[5] J. H. Dieterich, J. Geophys. Res. **84**, 2161 (1979).

[6] J. H. Dieterich, J. Geophys. Res. **84**, 2169 (1979).

[7] J. R. Rice, Pure Appl. Geophys. **121**, 443 (1983).

[8] A. L. Ruina, J. Geophys. Res. **88**, 359 (1983).

[9] F. Heslot, T. Baumberger, B. Perrin, B. Caroli, and C. Caroli, Phys. Rev. E **49**, 4973 (1994).

[10] P. Berthoud, T. Baumberger, C. G'Sell, and J.-M. Hiver, Phys. Rev. B **59**, 14313 (1999).

[11] T. Baumberger, C. Caroli, B. Perrin, and O. Ronsin, Phys. Rev. E **51**, 4005 (1995).

[12] Y. F. Lim and K. Chen, Phys. Rev. E **58**, 5637 (1998).

[13] S. M. Rubinstein, G. Cohen, and J. Fineberg, Phys. Rev. Lett. **96**, 256103 (2006).

[14] R. Maboudian and C. Carraro, Annu. Rev. Phys. Chem. **55**, 35 (2004).

[15] M. P. de Boer, D. L. Luck, W. R. Ashurst, A. D. Corwin, J. A. Walraven, and J. M. Redmond, J. Microelectromech. Syst. **13**, 63 (2004).

[16] A. D. Corwin and M. P. d. Boer, J. Microelectromech. Syst. **18**, 250 (2009).

[17] G. M. Pharr, W. C. Oliver, and D. R. Clarke, J. Mater. Res. **6**, 1129 (1991).

[18] J. J. Sniegowski and M. P. de Boer, Annu. Rev. Mater. Sci. **30**, 299 (2000).

[19] B. N. J. Persson, *Sliding Friction—Physical Priniciples and Applications* (Springer, Berlin, 1998).

[20] M. G. Hankins, P. J. Resnick, P. J. Clews, T. M. Mayer, D. R. Wheeler, D. M. Tanner, and R. A. Plass, Proc. SPIE **4980**, 238 (2003).

[21] R. W. Carpick and M. Salmeron, Chem. Rev. **97**, 1163 (1997).

[22] F. Schreiber, Prog. Surf. Sci. **65**, 151 (2000).

[23] M. F. Linker and J. H. Dieterich, J. Geophys. Res. **97**, 4923 (1992).

[24] L. Bureau, T. Baumberger, and C. Caroli, Eur. Phys. J. E **8**, 331 (2002).

[25] A. D. Corwin and M. P. de Boer, Appl. Phys. Lett. **84**, 2451 (2004).

[26] B. D. Jensen, M. P. de Boer, N. D. Masters, F. Bitsie, and D. A. LaVan, J. Microelectromech. Syst. **10**, 336 (2001).

[27] H. Yoshizawa and J. Israelachvili, J. Phys. Chem. **97**, 11300 (1993).

[28] K. Tuck, A. Jungen, A. Geisberger, M. Ellis, and G. Skidmore, ASME J. Eng. Mater. Technol. **127**, 90 (2005).

[29] S. M. Rubinstein, G. Cohen, and J. Fineberg, Nature (London) **430**, 1005 (2004).

[30] D. B. Asay, M. T. Dugger, J. A. Ohlhausen, and S. H. Kim, Langmuir **24**, 155 (2008).